Published in final edited form as:

Cancer Res. 2019 October 01; 79(19): 5034–5047. doi:10.1158/0008-5472.CAN-19-0880.

AMPK alpha-1 intrinsically regulates the function and differentiation of tumor myeloid-derived suppressor cells

Jimena Trillo-Tinoco[1], **Rosa A. Sierra**[1], **Eslam Mohamed**[1], **Yu Cao**[1], **Álvaro de Mingo-Pulido**[1], **Danielle L. Gilvary**[1], **Carmen M. Anadon**[1], **Tara Lee Costich**[1], **Sheng Wei**[1], **Elsa R. Flores**[2,3,4], **Brian Ruffell**[1,5], **José R. Conejo-Garcia**[1], **Paulo C. Rodriguez**[1,*]

[1]Department of Immunology, H. Lee Moffitt Cancer Center and Research Institute. 12902 Magnolia Dr. Tampa, FL 33612 USA.

[2]Department of Molecular Oncology, H. Lee Moffitt Cancer Center and Research Institute. 12902 Magnolia Dr. Tampa, FL 33612 USA.

[3]Department of Cutaneous Oncology, H. Lee Moffitt Cancer Center and Research Institute. 12902 Magnolia Dr. Tampa, FL 33612 USA.

[4]Cancer Biology and Evolution Program, H. Lee Moffitt Cancer Center and Research Institute. 12902 Magnolia Dr. Tampa, FL 33612 USA.

[5]Department of Breast Oncology. H. Lee Moffitt Cancer Center and Research Institute. 12902 Magnolia Dr. Tampa, FL 33612 USA.

Abstract

Myeloid-derived suppressor cells (MDSC) represent a primary mechanism of immune evasion in tumors and have emerged as a major obstacle for cancer immunotherapy. The immunoinhibitory activity of MDSC is tightly regulated by the tumor microenvironment (TME) and occurs through mechanistic mediators that remain unclear. Here, we elucidated the intrinsic interaction between the expression of AMP-activated protein kinase alpha (AMPKα) and the immunoregulatory activity of MDSC in tumors. AMPKα signaling was increased in tumor-MDSC from tumor-bearing mice and ovarian cancer patients. Transcription of the Ampkα1-coding gene, *Prkaa1*, in tumor-MDSC was induced by cancer cell-derived granulocyte-monocyte colony-stimulating factor (GM-CSF) and occurred in a Stat-5-dependent manner. Conditional deletion of *Prkaa1* in myeloid cells, or therapeutic inhibition of Ampkα in tumor-bearing mice, delayed tumor growth, inhibited the immunosuppressive potential of MDSC, triggered anti-tumor $CD8^+$ T-cell immunity, and boosted the efficacy of T-cell immunotherapy. Complementarily, therapeutic stimulation of AMPKα signaling intrinsically promoted MDSC immunoregulatory activity. In addition, *Prkaa1* deletion antagonized the differentiation of monocytic-MDSC (M-MDSC) to macrophages, and re-routed M-MDSC, but not granulocytic-MDSC (PMN-MDSC), into cells that elicited direct anti-tumor cytotoxic effects through nitric oxide synthase 2 (Nos2)-mediated actions. Thus, our results demonstrate the primary role of AMPKα1 in the immunosuppressive effects induced by tumor-

[*]**Correspondence:** Paulo C. Rodriguez, PhD. H. Lee Moffitt Cancer Center and Research Institute. Department of Immunology. 12902 Magnolia Dr. MRC-Annex 2067E. Tampa, FL 33612. Phone: 813-745-1457. Paulo.Rodriguez@Moffitt.org.

Disclosure of conflict of interest: The authors declare no potential conflicts of interest.

MDSC, and support the therapeutic use of AMPK-inhibitors to overcome MDSC-induced T-cell dysfunction in cancer.

Keywords

MDSC; AMPKα1; Tumor immunity; Nos2; nitric oxide

Introduction

"Emergency" myelopoiesis is characterized by an elevated production of myeloid precursors in the bone marrow as a response to acute infection or injury (1). During this process, monocytic and granulocytic cells actively participate in the elimination of agents through direct cytotoxic events and activation of T, B, and NK cells. However, this physiological process is de-railed in cancer, resulting in a chronic production of myeloid precursors that inhibit the development of protective anti-tumor immunity and support the formation, growth, and metastasis of tumors (2). These immunoregulatory immature myeloid cell populations are referred as myeloid-derived suppressor cells (MDSC) and are divided into "early stage" (e-MDSC), monocytic (M-MDSC) and granulocytic (PMN-MDSC) subsets (3). MDSC represent a key mechanism for the evasion of protective anti-tumor T-cell immunity and a significant obstacle for the development of effective therapies against cancer (4). Despite their undeniable relevance, there are no effective clinical therapies to permanently overcome the immunoregulatory effects of MDSC in cancer patients (5). This can be explained in part by the exaggerated myelopoiesis, the redundancy of the regulatory pathways, and the high plasticity of MDSC in individuals with tumors (5).

The exposure of MDSC to the tumor microenvironment (TME) potentiates their ability to thwart protective anti-tumor immunity through the induction of multiple pathways, including the expression of Arginase I and Nitric oxide synthase 2 (Nos2); and the release of reactive oxygen species (ROS) and peroxynitrite (PNT) (6). Also, the TME drives differentiation of M-MDSC into tumor-associated macrophages (TAM) (7-9). Production of several TME-related factors such as GM-CSF, G-CSF, and IL-6, activate interconnected signaling pathways that control MDSC survival, immunosuppression, and differentiation (4). However, the precise signaling mediators whereby the TME controls MDSC-related immune suppression remain unclear.

AMP-activated protein kinase (AMPK) is a heterotrimeric complex highly conserved from yeast to animals and comprises a catalytic subunit (AMPKα1 or 2) and two regulatory subunits (AMPKβ and γ) that function as a metabolic sensor to maintain energy homeostasis in stressed cells (10). Myeloid cells preferentially express AMPKα1 rather than AMPKα2 (11, 12). AMPK activity is regulated by an elevated AMP/ATP ratio and other stress mediators in the TME, and is highly dependent on its expression and phosphorylation (13, 14). Upon activation, AMPK promotes metabolic plasticity through multiple processes including the promotion of fatty acid oxidation and mitochondrial homeostasis (15-17), which have been recently reported as major drivers of the immunoregulatory activity of myeloid cells in tumors (18). Although the role of AMPK is well established in cancer cells,

the intrinsic effect of AMPK in the modulation of MDSC in tumors remains controversial. Initial reports showed that pharmacological activation of AMPK blocked MDSC function in tumors (19-25), while additional investigations indicated that AMPK promoted MDSC activity (26-28). Development of conditional AMPK-deficient models will enable precise elucidation of the actions of AMPK signaling in tumor-associated MDSC.

In this study, we sought to dissect the interaction between the expression of AMPKα1 and the immunoregulatory effects triggered by MDSC in tumors. Conditional deletion of the Ampkα1-coding gene, *Prkaa1* in myeloid cells, or inhibition of Ampkα in tumor-bearing mice, impaired MDSC suppressive activity, blunted M-MDSC-to-macrophage differentiation, and de-railed M-MDSC into anti-tumor cytotoxic cells by Nos2-dependent pathways. These results demonstrate the major role of AMPKα1 in the immunosuppressive activity of MDSC in tumors and provide new strategies for the therapeutic inhibition of MDSC-driven T-cell dysfunction in cancer.

Material and Methods

Cell Lines and Animals

Cell lines Lewis lung carcinoma (LLC), EL4 thymoma, B16-F10 melanoma (ATCC), MCA-38 colon carcinoma (Kerafast), B16-GM-CSF melanoma (Dr. Esteban Celis, Augusta University), and ID8-*Defb29/Vegf-a* ovarian carcinoma (29, 30) (Dr. Conejo-Garcia, Moffitt) were cultured in RPMI-1640 (Lonza) supplemented with 10% fetal calf serum (Gemini), 25 mM Hepes, 4 mM L-glutamine, and 100 U/ml of penicillin-streptomycin (Invitrogen). B16 cells were transduced with lentivirus coding for non-targeting shRNA control or *Csf2*-targeting shRNA (Dharmacon, RHS6848 and RMM3981–200805373) and selected in 2 μg/ml puromycin-containing medium. Tumor cell lines were authenticated on May 2018 and validated to be mycoplasma-free using an ATCC detection kit in October 2018. All studies were conducted with cells within the first 5 passages. C57BL/6J mice (6 to 8-wk-old) were from Envigo. Myeloid cell-conditional *Prkaa1*-deficient ($Prkaa1^{KO}$) mice were developed after breeding *Prkaa1 loxP/loxP* ($Prkaa1^{flox}$) mice with those carrying Lysozyme promoter-driven *Cre* recombinase (both from the Jackson Laboratories). Pmel-1 mice and *Nos2*-deficient mice were from the Jackson Laboratories. Mice were s.c. injected with LLC, EL4, MCA-38, B16, or B16-GM-CSF cells, as reported (31). MMTV-PyMT breast tumor cells from transgenic animals (Dr. Ruffell, Moffitt) were implanted orthotopically in the mammary fat pads, and ID8-*Defb29*/*Vegf-a* tumor cells were injected i.p. and mice evaluated until they reached a weight gain greater than 30% (29). Tumor volume was tested using calipers and calculated using the formula [$(\text{small diameter})^2 \times (\text{large diameter}) \times 0.5$]. All studies using animals were approved by the Moffitt-IACUC and followed Moffitt's Comparative Medicine facility guidelines.

Patient Population

A tissue microarray (TMA, Moffitt Cancer Center) was available for 79 de-identified and pathologically confirmed high-grade advanced serous epithelial ovarian carcinoma tumors and 10 healthy ovary or fallopian tube tissues. Also, peripheral blood from de-identified patients with advanced ovarian carcinoma and healthy donors was obtained from a tissue

repository established by Dr. Conejo-Garcia (Moffitt Cancer Center). Moreover, we obtained de-identified mobilized peripheral blood stem cells (PBSC) from healthy donors for hematopoietic stem cell transplantation (HSCT) (Georgia Cancer Center Biorepository). Additionally, T-cells were isolated from de-identified buffy coats from healthy blood donors (One-Blood). Studies using de-identified human samples were covered through an exempt-approved Institutional Review Board (IRB) protocol and were developed following the Regulatory Affairs Committee guidelines at Moffitt Cancer Center. Investigators and biorepository facilities obtained informed written consent forms from the de-identified subjects.

Reagents

For modulation of AMPKα activity, MDSC were treated with 5-Aminoimidazole-4-carboxamide 1-β-D-ribofuranoside (Aica-R, 200 μM, Millipore), Metformin (10 mM, Millipore), or Dorsomorphin-Compound C (CC, 5 μM, Cayman). Moreover, LLC-bearing mice received CC (15 mg/kg, i.t.), Metformin (150 mg/kg, i.p.), or Aica-R (0.5 mg/kg, i.p.) 9 days post-tumor injection and continued to be treated daily until tumor endpoint. For *in vitro* studies inhibiting Nos2, we used L-NG-Monomethylarginine (L-NMMA, 500 μM, Cayman) and Lysine-dihydrochloride (L-NIL, 300 μM, Cayman); whereas for *in vivo* assays, LLC-bearing mice were treated daily starting at day 0 of tumor injection with 20 mg/kg L-NIL (Cayman, i.p.). Human IL-6, mouse granulocyte-monocyte colony stimulating factor (GM-CSF) and mouse granulocyte-colony stimulating factor (G-CSF) were from Gemini. Human GM-CSF was from eBioscience. Thioglycolate broth from Sigma-Aldrich was prepared at 4% in water, autoclaved, and stored in dark for 2 weeks before i.p. injection. To test the role of GM-CSF in TES-treated MDSC, we utilized blocking antibodies against mouse-GM-CSF (5 μg/ml, Clone MP1022E9) and/or mouse-GM-CSF receptor α (1 μg/ml, Clone 698423, R&D systems). Rat IgG2a isotype (Clone 2A3, BioXcell) was used as control.

Flow cytometry

Surface staining was performed followed labeling with viability Zombie dyes (Biolegend) and purified anti-mouse CD16/CD32 antibodies (Clone 2.4G2, BD Biosciences). The following antibodies were used: CD45-BV785 or BV421 (Clone 30-F11, Biolegend), CD11b-FITC or BV421 (Clone M1/70, Biolegend), Gr1-PE-Cy5 or PE/Dazzle594 (Clone RB6–8C5, Biolegend), F4/80-APC-AF700 (Clone BM8, Biolegend), Ly6G-APC (Clone 1A8, Tonbo), Ly6C-PE or FITC (Clone AL-21, BD Biosciences). For intracellular detection of Nos2 (Clone CXNFT, eBioscience), AMPKα (Clone F6, Cell Signaling Technologies), or phospho-AMPKα (Thr172) (Rabbit polyclonal 40H9, Cell Signaling Technologies), tumor cell suspensions or MDSC were cultured for 6 hours in the presence of GolgiStop (0.8 μl/ml, BD Biosciences) plus LPS (1 μg/ml, Sigma-Aldrich) for Nos2; or GolgiStop (0.8 μl/ml), phorbol myristate acetate (PMA, 750 ng/mL, Sigma-Aldrich) and ionomycin (50 μg/mL, Sigma-Aldrich) for total and phospho AMPKα. Intracellular staining was completed using Cytofix/ Cytoperm and Perm-Wash buffers (BD Biosciences). T-cell proliferation was detected using Carboxyfluorescein succinimidyl ester (CFSE) (Molecular Probes). T-cells were labeled with 1 μM CFSE at 37°C for 15 minutes. For T-cell:MDSC co-cultures (1:0.5 ratio, unless specified), T-cells were primed with plate-bound anti-CD3 plus anti-CD28 (1

μg/ml each, Clones 145–2C11 and 37.51 from BD Biosciences) and cultured with MDSC or TAM for 72 hours. For human T-cell:MDSC (1:2 ratio) co-cultures, T-cells were primed with soluble anti-CD3 (1 μg/ml, clone OKT3, Thermo-Fisher) and anti-CD28 (0.5 μg/ml, clone L293, BD Biosciences) in 96 well-plates bound with 10 μg/ml goat anti-mouse (KPL). Results are expressed as percentage of proliferating T-cells, determined by the dilution of CFSE fluorescence compared with non-stimulated T-cells. Murine MDSC were identified by flow cytometry as: MDSC ($CD45^+$ $CD11b^+$ $Gr1^+$ $F4/80^{neg}$), PMN-MDSC ($CD45^+$ $CD11b^+$ $Gr1^+$ $Ly6C^{low}$ $Ly6G^+$), and M-MDSC ($CD45^+$ $CD11b^+$ $Gr1^+$ $Ly6C^{high}$ $Ly6G^{neg}$) (3); while TAM were recognized as $CD45^+$ $CD11b^+$ $Gr1^{neg}$ $F4/80^+$. Cells resembling human MDSC were identified by flow cytometry as e-MDSC ($CD45^+$ $CD33^+$ HLA-$DR^{neg/low}$ $CD14^{neg}$ $CD15^{neg}$), PMN-MDSC ($CD45^+$ $CD33^+$ HLA-$DR^{neg/low}$ $CD15^+$ $CD14^{neg}$), and M-MDSC ($CD45^+$ $CD33^+$ HLA-$DR^{neg/low}$ $CD14^+$ $CD15^{neg}$) (3). Cells were collected using a CytoFlex flow cytometer (Beckman Coulter). Analyses were performed using the FlowJo V10 (FlowJo).

Western Blot

Whole cellular lysates were electrophoresed in 8 or 10% Tris-Glycine gels (Novex-Invitrogen), transferred into nitrocellulose membranes (Bio-Rad), and immunoblotted with antibodies against phospho-Ampkα (Thr172) (Rabbit polyclonal 40H9, Cell Signaling Technologies), Ampkα (Clone F6, Cell Signaling Technologies), Nos2 (Clone 54/iNOS, BD Biosciences), Arginase I (Goat polyclonal N20, Santa Cruz Biotechnologies), Phospho-Stat-5 (Tyr694) (Rabbit polyclonal D47E7, and Clone 14H2, Cell Signaling Technologies), Stat-5 (Rabbit polyclonal D2O6Y, Cell Signaling Technologies), Stat-5a (Rabbit monoclonal E289, Abcam), Stat-5b (Rabbit polyclonal AF1584, R&D systems), or Vinculin (Clone hVIN-1, Sigma-Aldrich) (All at 1:1000). Horseradish peroxidase linked anti-mouse IgG, anti-rabbit IgG (both from GE Healthcare), or anti-goat IgG (Santa Cruz Biotechnologies) were used as secondary antibodies and used at 1:5000. Membrane-bound immune complexes were detected using ECL-Western Blot Substrate Reagent (Thermo-Fisher) and images acquired using a Chemidoc Imaging System and analyzed using the Image-Lab software (Bio-Rad).

Isolation of cells and development of MDSC

$CD3^+$ T-cells were isolated from spleen and lymph nodes of C57BL/6 mice, or from purchased human buffy-coat units (One-Blood) using T-cell negative selection kits (MagniSort, Invitrogen). Purity ranged between 95% and 99% as tested by flow cytometry. MDSC were isolated from cellular suspensions of spleen or tumors digested with DNase I and Liberase (Roche) (31). Also, MDSC, M-MDSC, PMN-MDSC, and TAM were isolated by fluorescence-activated cell sorting. Splenic-MDSC were cultured in the presence of 20 ng/ml GM-CSF or 20% LLC-tumor explants (TES), prepared from filtered supernatants of primary LLC tumors cultured overnight (1×10^7/ml). Also, splenic-MDSC (2×10^6) from $CD45.1^+$ mice bearing EL4 tumors (~2000 mm^3) were transferred into the peritoneal cavity of $CD45.2^+$ mice: 1) bearing established i.p. EL4 tumors ($CD45.2^+$); 2) undergoing thioglycolate-induced peritonitis for 12 hours; or 3) naïve controls. Peritoneal $CD45.1^+$ cells were sorted 18 hours later. *In vitro* developed human MDSC were generated from $CD34^+$ $CD33^+$ PBSC of healthy donors for HSCT. Precursors were cultured for 7 days with GM-

CSF and IL-6 (20 ng/ml each) and different AMPKα modulating agents or 30% tumor-conditioned medium from renal cell carcinoma 786–0 cells (hTES) (31).

Depletion of CD8$^+$ T-cells or MDSC and Adoptive Transfer

To eliminate CD8$^+$ T-cells or MDSC-like cells, LLC-bearing mice were treated with 400 μg anti-CD8 (clone 53.6.72, BioXcell) or 250 μg anti-Gr1 (clone RB6–8C5, BioXcell), respectively. Maintenance i.p. doses of the depleting antibodies were given every 3rd day until tumor endpoint. In MDSC co-injection studies, 1×10^6 tumor-MDSC, PMN-MDSC, or M-MDSC from *Prkaa1*^{flox} and *Prkaa1*^{KO} mice bearing LLC tumors were co-injected s.c. with 1×10^6 LLC cells. For adoptive T-cell therapy (ACT), mice bearing B16 tumors for 6 days, received ACT with 1×10^6 negatively sorted CD8$^+$ pmel T-cells pre-activated for 48 hours with $gp100_{25–33}$ (AnaSpec). Ten days after pmel transfer, lymph nodes were activated for 24 hours with 1 μg/ml $gp100_{25–33}$ and tested for IFNγ expression using EliSpot (R&D systems).

Immunofluorescence

Formalin fixed paraffin embedded baked TMA sections were transferred to a BOND RX (Leica Biosystems) and staining performed using an automated OPAL-IHC system (PerkinElmer). Briefly, slides were treated with the PerkinElmer blocking buffer for 10 min and incubated with the specific primary antibodies, followed by OPAL-HRP polymer and one OPAL fluorophore. Individual antibody complexes were stripped after each round of detection and DAPI applied as the last staining. Auto-fluorescence slides (negative control) included primary and secondary antibodies, omitting the OPAL fluorophores. Slides were imaged with a Vectra®3 Automated Quantitative Pathology Imaging System. Cells resembling MDSC were identified by imaging as M-MDSC (Pan-cytokeratin^{neg} HLA-DR$^{neg/low}$ CD14$^+$ CD15^{neg}) or PMN-MDSC (Pan-cytokeratin^{neg} HLA-DR$^{neg/low}$ CD15$^+$ CD14^{neg}). Multi-layer TIFF images were exported from InForm (PerkinElmer) into HALO (Indica Labs) for quantitative analysis. Each fluorophore was assigned to a dye color and positivity thresholds determined visually per marker based on intensity thresholds normalized for exposure (counts/2 bit depth x exposure time x gain x binning area). Cell segmentation results from each core were analyzed using FCS Express 6 Image Cytometry (De Novo software).

Cytotoxicity assay

CFSE-labeled EL4 cells were co-cultured with M-MDSC or PMN-MDSC (ratio 1:5) (31), and in the presence or the absence of L-NMMA or L-NIL. EL4 cells were also co-cultured with M-MDSC from tumor-bearing mice treated with L-NIL, or from *Nos2*^{KO} or wildtype mice treated with CC. After 24 hours of co-culture, EL4 cells were stained with Violet Zombie dye and then fixed with Cytofix buffer (BD Biosciences). Percentage of cell-dead within the EL4-CFSE$^+$ cells was measured by flow cytometry.

Quantitative real time-PCR (RT-PCR) and Multiplex arrays

Total RNA was extracted using TRIzol (Life Technologies), according to the manufacturer's instructions. RNA was reversely transcribed using the Verso cDNA synthesis Kit

(Invitrogen). RT-PCR analyses were performed with SYBGreen (Bio-Rad) using primers synthetized by Integrated DNA Technologies (IDT, Coralville, IA). The following primers were used: *Gapdh*: forward 5'-CTGCCCAGAACATCATCCCT-3', reverse 5'-ACTTGGCAGGTTCTCCAGG-3'; *Prkaa1*: forward 5'-GTCAAAGCCGACCCAATGATA-3', reverse 5'-CGTACACGCAAATAATAGGGGTT-3'. Fold-change expression was calculated by comparing the RNA values from experimental samples relative to the endogenous *Gapdh* control, compared with the results obtained from a pooled sample. Thus, fold change $=2^{-\Delta(\Delta CT),}$ where ΔCT = CT (*Prkaa1*) – CT (*Gapdh*); and Δ(ΔCT) = ΔCT (*Prkaa1*) – ΔCT (*Gapdh* pool of all samples). RT^2 profiler cancer inflammation and immunity crosstalk PCR array (Qiagen) was done in tumor-MDSC from LLC-bearing *Prkaa1*^{flox} and *Prkaa1*^{KO} mice, following the vendor's suggestions.

Chromatin immunoprecipitation assay

Chromatin immunoprecipitation (ChIP) assays were done using a SimpleChip kit (Cell Signaling Technologies), following the vendor's recommendations. Briefly, digested and cross-linked chromatin was prepared from 4×10^6 tumor-MDSC or splenic-MDSC treated or not with GM-CSF or TES for 72 hours, followed by immunoprecipitation with antibodies against phospho-Stat-5, Histone H3, or rabbit IgG (Cell Signaling Technologies). Eluted and purified DNA was analyzed by qPCR with the following primers targeting the *Prkaa1* promoter: forward 5'-AGCTTTCTTCCCCCTGAATACTTT-3'; reverse 5'-CTCCTAGTTCCATATTCTGGCT-3'. Primers against *Rpl30* promoter provided in the kit were used as housekeeping control.

Statistical Analysis

Two-tailed unpaired Student's *t*-test was used for most of the statistical analyses using the Prism software (Graph-Pad). Also, analyses of survival were assessed through Mantel-Cox test. P value of <0.05 was considered statistically significant. Specific statistical test results are indicated in each figure: *, $p<0.05$; **, $p<0.01$ ***, $p<0.001$.

Results

AMPKα induction in tumor-exposed MDSC.

To understand the potential interaction between AMPKα signaling and the regulatory function of tumor-associated MDSC, we monitored the expression of Ampkα and the immunosuppressive activity of tumor and splenic-MDSC ($CD11b^+$ $Gr1^+$) from mice bearing LLC tumors; and splenic PMN, monocytes, and immature myeloid cells ($CD11b^+$ $Gr1^+$, iMC) from mice without tumors. An increased expression of total and phospho-Ampkα and an augmented ability to impair T-cell proliferation were found in tumor-MDSC, compared to splenic-MDSC from LLC-bearing mice or iMC from tumor-free mice (Figure 1A-B). Also, an elevation of total and phospho-Ampkα was noted in tumor-MDSC from B16, EL4, or MMTV-PyMT-bearing mice, compared to splenic controls (Suppl. Figure 1A). Notably, the Ampkα signaling activation in tumor-MDSC occurred in PMN-MDSC and M-MDSC (Suppl. Figure 1B). Next, we studied whether AMPKα signaling was also heightened in human-MDSC infiltrating tumors. Using high-resolution automated multispectral imaging, we assessed the expression of phospho-AMPKα in a TMA made from 79 patients with

advanced high-grade serous ovarian tumors and 10 healthy ovary controls. Higher levels of phospho-AMPKα were noticed in cells resembling M-MDSC (Pan-cytokeratin^{neg} HLA-DR$^{neg/low}$ CD14^{+} CD15^{neg}) from ovarian tumors, compared to cellular counterparts from healthy ovaries (Figure 1C). However, analysis of phospho-AMPKα in tumor PMN-MDSC could not be completed as limited numbers of Pan-cytokeratin^{neg} HLA-DR$^{neg/low}$ CD14^{neg} CD15^{+} cells were found in ovarian tumors or healthy tissues (Figure 1C, Suppl. Figure 1C). To further explore the activation of AMPKα in MDSC subsets, we then examined the expression of phospho-AMPKα in peripheral blood from ovarian cancer patients and healthy controls by flow cytometry. Higher phospho-AMPKα levels were found in cells resembling e-MDSC, PMN-MDSC, and M-MDSC (3) from advanced ovarian cancer patients, compared to controls (Figure 1D), indicating the active AMPKα signaling in circulating MDSC from ovarian cancer patients.

Next, we investigated the contribution of the TME in the induction of Ampkα in MDSC by treating splenic-MDSC with LLC tumor explants (TES). Upregulation of total and phospho-Ampkα, higher levels of the MDSC-inhibitory factors Arginase I and Nos2, and elevated T-cell immunoregulatory activity, were noticed in TES-treated MDSC, compared to controls (Figure 1E-F). To elucidate the specific effect of the TME *vs.* overall inflammation in the induction of Ampkα in MDSC, we transferred CD45.1^{+} splenic-MDSC into the peritoneum of CD45.2^{+} mice previously injected with peritoneal EL4 tumors or the inflammatory agent thioglycolate. CD45.1^{+} cells were sorted 18 hours later and tested for the expression of Ampkα and the ability to impair T-cell proliferation. Higher levels of total and phospho-Ampkα and an augmented capacity to block T-cell proliferation were noted in MDSC previously transferred into EL4 tumors, compared to those from chemically-induced peritonitis or untreated mice (Figure 1G-H). Thus, results indicate the driving effect of the TME in the induction of AMPKα in MDSC and the potential interaction between AMPKα and MDSC activity.

TME-associated GM-CSF triggers Ampkα expression in MDSC through Stat-5.

We aimed to identify the TME factors driving Ampkα expression in tumor-MDSC. We focused on the role of GM-CSF as its production in the TME plays a primary role in MDSC activity (32, 33). Treatment of splenic-MDSC with GM-CSF induced the expression of total and phospho-Ampkα and enhanced their ability to blunt T-cell proliferation (Figure 2A-B, Suppl. Figure 2A-C). Moreover, blockade of GM-CSF and GM-CSF receptor α partially blunted the upregulation of Ampkα and the immunosuppressive activity of TES-treated MDSC (Figure 2C-D, Suppl. Figure 2D), suggesting the effect of the TME-associated GM-CSF in the induction of Ampkα in MDSC. Next, we tested the role of the cancer cell-derived GM-CSF in the induction of Ampkα in MDSC. Lower expression of total and phospho-Ampkα and reduced immunosuppressive activity were found in tumor-MDSC from mice bearing GM-CSF-silenced B16 tumors compared to controls (Figure 2E-F, Suppl. Figure 2E-F). In agreement, higher levels of total and phospho-Ampkα and augmented ability to impair T-cell proliferation were found in splenic-MDSC from mice carrying B16 cells overexpressing GM-CSF (B16-GM-CSF) (Figure 2G-H, Suppl. Figure 2G), indicating the role of cancer cell-derived GM-CSF in the induction of AMPKα in MDSC.

Next, we sought to identify the intracellular mediators by which GM-CSF promoted *Prkaa1* transcription. Our recent report showed the interaction between GM-CSF production in the TME and the phosphorylation of Stat-5 in tumor-MDSC (18). Elevated levels of total Stat-5, Stat-5a, Stat-5b; and augmented expression and endogenous binding of phospho-Stat-5 to the *Prkaa1* promoter were found in tumor-infiltrating MDSC compared to splenic-MDSC or iMC (Figure 2I-J, Suppl. Figure 2H), and in splenic-MDSC treated with TES or GM-CSF (Figure 2K-L, Suppl. Figure 2I). Notably, the inhibition of Stat-5 through Pimozide impaired the induction of *Prkaa1* mRNA and Ampkα protein in GM-CSF or TES-treated splenic-MDSC (Figure 2M). Thus, our results suggest the primary role of TME-associated GM-CSF and intrinsic signaling through Stat-5 in the induction of Ampkα in tumor-MDSC.

AMPKα modulation regulates the immunosuppressive activity of tumor-MDSC.

We tested the therapeutic effects of the inhibition of AMPKα in tumor-bearing mice. Delayed tumor growth and alterations in tumor-MDSC, including impaired immunosuppressive activity, diminished expression of the immune inhibitory factor Arginase I, and increased Nos2 levels, were found LLC-bearing mice treated with the AMPK inhibitor, CC, compared to controls (Figure 3A-C). Because MDSC activity depends on tumor burden, we further tested the intrinsic effects of the modulation of AMPKα in the activity of human MDSC developed from myeloid precursors (Suppl. Figure 3) (18, 34), after exposure to effective doses of the AMPK agonists, Aica-R and Metformin, or the AMPK inhibitor, CC (Figure 3D). In agreement with the immune suppressive role of AMPK in MDSC, we observed a higher immunoregulatory activity in Aica-R pre-treated MDSC and reduced immunoinhibitory potential in CC-conditioned MDSC, compared to controls, which correlated with corresponding changes in phospho-AMPKα levels (Figure 3D-E). Also, despite the elevation of phospho-AMPKα in Metformin-treated MDSC, we found a decrease in their immunosuppressive potential (Figure 3D-E), suggesting opposite effects of the AMPK agonists, Aica-R and Metformin, in human MDSC. To further evaluate possible off-target effects of the AMPK agonists, we repeated the treatments in splenic-MDSC from myeloid cell-conditional Ampkα1-null (*Prkaa1*^{KO}) mice, created after crossing *Prkaa1*^{flox} mice with those carrying Lysozyme-driven *Cre* recombinase. *Prkaa1* deletion antagonized the increased immune regulatory activity observed in TES or Aica-R-exposed MDSC, without impacting Metformin-treated MDSC (Figure 3F), suggesting that TES and Aica-R, but not Metformin, modulate MDSC regulatory activity in an Ampkα1-dependent manner. Furthermore, we tested the role of myeloid cell-Ampkα1 in the tumor effects induced by Aica-R or Metformin treatments in mice. *Prkaa1* deletion overcame the slight potentiation of tumor growth induced by Aica-R treatment in mice (Figure 3G). Conversely, the delayed tumor growth noticed in LLC-bearing mice treated with Metformin was not altered by deletion of *Prkaa1* in myeloid cells (Figure 3H), showing that Aica-R, but not Metformin, induced anti-tumor effects in a myeloid cell Ampkα-related manner.

Prkaa1 deletion impairs MDSC suppressive activity and differentiation into TAM.

To determine the specific contribution of Ampkα1 in myeloid cells in tumor growth, we used myeloid cell-conditional *Prkaa1*^{KO} mice. A delay in the growth of several tumors, including LLC, MCA-38, EL4, B16, and MMTV-PyMT was noticed in *Prkaa1*^{KO} mice, compared to *Prkaa1*^{flox} controls (Figure 4A). Also, extended survival was found in LLC,

EL4, B16, and ID8-*Defb29/Vegf-a* bearing *Prkaa1*^{KO} mice, compared to controls (Suppl. Figure 4A). Furthermore, an evident decrease in the T-cell suppressive potential was noticed in tumor-MDSC from *Prkaa1*^{KO} mice, compared to those from control mice (Figure 4B), which correlated with a lower expression of Arginase I and a surprising upregulation of Nos2 (Figure 4C). Additionally, gene transcript assessment showed increased levels of *Nos2*, *Il12a*, *Tlr4*, *Cxcl1*, and *Myd88*; and lower *Aicda*, *Tnfsf10*, and *Cxcl10* mRNA expression in tumor-MDSC from *Prkaa1*^{KO} mice compared to controls (Suppl. Figure 4B-C). Because gene targeting using Lysozyme-*Cre* recombinase does not specifically affect MDSC, we then distinguished the effect of the deletion of *Prkaa1* on the two most frequent myeloid subsets in LLC tumors, MDSC and TAM. Increased accumulation of cells resembling MDSC, PMN-MDSC, and M-MDSC; and lower frequency of TAM were found in tumors from *Prkaa1*^{KO} mice compared to controls (Figure 4D). Because M-MDSC represent a primary source for TAM expansion in the TME (7-9), we tested the effect of Ampkα in the M-MDSC-to-TAM differentiation. In accordance with the lower frequency of TAM in tumors from *Prkaa1*^{KO} mice, a diminished differentiation of TES-conditioned M-MDSC to macrophages was observed upon *Prkaa1* deletion (Figure 4E). Also, we compared the role of Ampkα1 in the T-cell-suppressive activity of MDSC *vs.* TAM. *Prkaa1* deletion impacted the immunoregulatory activity and the levels of Arginase I in tumor-MDSC, while promoting Nos2 expression. However, these effects were not observed in TAM (Figure 4F-G). Interestingly, the low immunosuppressive activity of *Prkaa1*^{KO} MDSC from tumors was observed both in PMN-MDSC and M-MDSC (Figure 4F). Thus, results show the role of *Prkaa1* in the differentiation and immunoinhibitory function of tumor-MDSC, but not in TAM suppressive activity.

Conditional deletion of *Prkaa1* in MDSC primes anti-tumor T-cell responses.

We next sought to elucidate the role of T-cell immunity in the anti-tumor effects induced by the conditional deletion of *Prkaa1* in myeloid cells. In agreement with the role of Ampkα1 in the promotion of MDSC function, elevated frequency of $CD8^+$ T-lymphocytes and $CD8^+$ $CD44^+$ $CD69^+$ antigen-experienced T-cells was observed in tumors from *Prkaa1*^{KO} mice, compared to controls (Figure 5A-B). Moreover, depletion of $CD8^+$ T-cells restored tumor growth in *Prkaa1*^{KO} mice (Figure 5C). Next, we tested the impact of the MDSC-Ampkα1 in tumor-induced T-cell tolerance using an ACT model against the tumor-antigen gp100, in which activated anti-$gp100_{25–33}$ transgenic pmel T-cells were transferred into mice bearing B16 tumors. A significant delay in tumor growth and a higher frequency of IFNγ-expressing pmel T-cells were found in B16-bearing *Prkaa1*^{KO} mice undergoing ACT, compared to flox controls receiving the same amount of pmel T-cells (Figure 5D-E). Thus, results suggest the key role of MDSC-related Ampkα1 in tumor-induced T-cell dysfunction.

Prkaa1-deficient M-MDSC eliminate tumor cells in a Nos2-mediated manner.

To determine whether *Prkaa1* deletion transforms MDSC into cells that elicit anti-tumor actions, we eliminated MDSC using anti-Gr1 antibodies; and co-injected *Prkaa1*^{flox} mice with LLC cells and tumor-MDSC from *Prkaa1*^{KO} or flox mice (31). MDSC depletion restored tumor growth in *Prkaa1*^{KO} mice and delayed tumor progression in control mice (Figure 6A). Also, in agreement with the anti-tumor actions of *Prkaa1*^{KO} MDSC, delayed tumor growth was found after transfer of *Prkaa1*^{KO}-MDSC, compared to mice receiving

flox-MDSC (Figure 6B). Notably, *Prkaa1*^{KO}-MDSC triggered similar anti-tumor effects after transfer into immunodeficient *Rag*^{KO} mice (Figure 6C), indicating that *Prkaa1* deletion transforms MDSC into cells that potentially elicit direct tumor cytotoxicity. To further explore this possibility, we assessed the cytotoxic potential of tumor-MDSC subsets from flox and *Prkaa1*^{KO} mice on cultured EL4 tumor cells. *Prkaa1*^{KO}-M-MDSC showed enhanced ability to eliminate EL4 tumor cells, compared to *Prkaa1*^{KO}-PMN-MDSC or tumor-MDSC subsets from *Prkaa1*^{flox} mice (Figure 6D). Moreover, co-injection of LLC cells with *Prkaa1*^{KO} M-MDSC, but not with *Prkaa1*^{KO} PMN-MDSC, resulted in delayed tumor growth in both wildtype and *Rag*^{KO} mice (Figure 6E, Suppl. Figure 5), confirming the ability of *Prkaa1*^{KO} M-MDSC to induce direct anti-tumor effects. Interestingly, the increased anti-tumor cytotoxic activity of *Prkaa1*^{KO}-M-MDSC correlated with a higher expression of Nos2 (Figure 6F) and was completely inhibited after treatment with the Nos2 inhibitors, L-NMMA or L-NIL (Figure 6G), suggesting the impact of Nos2 in the anti-tumor cytotoxic actions induced by *Prkaa1*^{KO}-M-MDSC. Next, we elucidated whether the inhibition of Nos2 overcame the effects observed in *Prkaa1*^{KO} mice. Treatment of LLC-bearing *Prkaa1*^{KO} mice with the Nos2 inhibitor, L-NIL, partially restored tumor growth and ablated the ability of tumor-M-MDSC to kill tumor cells (Figure 6H-I). Accordingly, knockdown of *Nos2* in LLC-bearing mice partially prevented the anti-tumor effects and M-MDSC cytotoxic activity induced after treatment with CC (Figure 6J-K). Thus, the overall results indicate that knockdown of *Prkaa1* induced M-MDSC-like cells with the ability to elicit direct anti-tumor effects through Nos2-dependent pathways.

Discussion

Our study reveals a new role of AMPKα as a direct mediator of the immunosuppressive activity and differentiation of MDSC in tumors and suggests the therapeutic potential of inhibiting AMPK signaling as a strategy to restore protective myelopoiesis in cancer.

Upregulation and phosphorylation of AMPKα are key steps in the cellular adaptation to various stress conditions, including nutrient deprivation, elevation of intracellular AMP-ADP/ATP ratio, accumulation of reactive species, and hypoxia (10). Priming of AMPKα1 occurs through its phosphorylation by the liver-kinase-B1 (LKB1) and the calcium/calmodulin-dependent kinase kinase 2 (CAMKK2) (13, 14); and aims to restore energy homeostasis in stressed cells by inhibiting anabolic processes consuming ATP and by activating catabolic signals that generate ATP (15-17). Interestingly, stimulation of AMPK signaling in cancer cells has emerged as a key regulator of anti-tumor immune responses. Activation of AMPK by aerobic glycolysis in breast tumors promoted MDSC expansion through the production of G-CSF and GM-CSF (35). Also, rapidly proliferating cancer cells imposed nutrient competition and accumulation of multiple reactive metabolites, such as adenosine, that activated AMPK in tumor-associated myeloid cells (36). In contrast to the immunosuppressive effects of cancer cell-expressed AMPK, stimulation of AMPK in breast cancer tumors through the AMPK agonist, Metformin, endogenously induced phosphorylation and degradation of PD-L1, thereby promoting protective T-cell immunity (37). Thus, priming of AMPK signaling in malignant cells can activate both anti-tumor and pro-tumor responses.

Our results show that treatment of tumor-bearing mice with CC or conditional deletion of *Prkaa1* in myeloid cells blunted the immunoregulatory function of MDSC and improved protective T-cell immunity. Similarly, inhibition of AMPK by CC thwarted the expression of the immune inhibitory factor Arginase I in bone marrow-derived MDSC treated with GM-CSF and IL-6 (28). The immunoregulatory effects of AMPK are not restricted to MDSC. Indeed, previous reports described the role of AMPK in the activation of immunosuppressive phenotypes in macrophages and in the restriction of effector T-cell expansion in tumors (12, 38). In contrast to our argument that AMPK drives the tolerogenic actions of MDSC, treatment of tumor-bearing mice with the AMPK agonists Metformin, Phenformin, or OSU-53 exerted anti-tumor activities that correlated with a lower immunosuppressive function of MDSC (19-25). Conversely, additional studies showed that treatment of M-MDSC with Metformin promoted their immunosuppressive activity in allogeneic skin grafts (26); and enhanced MDSC response to the immunoinhibitory factor prostaglandin E_2 in models of doxorubicin-resistant tumors (27). The paradoxical effects induced by Metformin, and other AMPK activators, on the activity of MDSC could be explained by several possibilities, including the potential combined effects of the modulation of AMPK in different cellular populations in the TME, the levels of the nutritional stress and AMPK signaling in different tumor models, and potential off-target effects (39). In agreement with the AMPKα-independent effects of Metformin (39-41), our results showed that the intrinsic effects induced by Metformin in MDSC were not responsive to the deletion of *Prkaa1*. Similarly, the anti-tumor effects induced by Metformin in LLC-bearing mice were not impacted by the elimination of *Prkaa1* in myeloid cells. Because Metformin has been reported to modulate additional targets, including mTORC1, Protein Kinase A and mitochondrial Glycerophosphate Dehydrogenase (39-41), development of therapeutic models in specific deficient mice for these targets will enable to establish the precise mechanism of action of Metformin in MDSC.

Previous results demonstrated the driving effect of the TME in the differentiation of M-MDSC into TAM (7-9). Our findings show that deletion of *Prkaa1* antagonized M-MDSC-to-TAM differentiation, which agrees with a recent report highlighting the role of Ampkα1 in the differentiation of atherosclerosis-linked monocytes-to-macrophages (42). Notably, although AMPK has been previously shown to control anti-inflammation signals in macrophages (11, 12), we did not observe alterations in the immunosuppressive activity or changes in the levels of Arginase 1 or Nos2 in $Prkaa1^{KO}$ TAM, indicating that *Prkaa1* deletion impairs differentiation of M-MDSC-to-TAM, but not TAM immunoregulatory activity. Mechanistic mediators for the M-MDSC-to-TAM differentiation process include the induction of the hypoxia-inducible factor-1 alpha (HIF-1α), the decreased transcriptional activity of Stat-3, the activation of the RAR-related orphan receptor C (RORC1), Notch, or Aryl hydrocarbon receptor (AhR), and the signaling mediated by M-CSF and GM-CSF receptors (8, 9, 43-45). Although the mechanisms by which AMPKα1 regulates M-MDSC-to-TAM differentiation remain to be elucidated, it is conceivable that the effect of TME-derived GM-CSF in the transcriptional induction of *Prkaa1*, combined with relevant stress mediators in the TME such as hypoxia or nutrient deprivation, could induce activation of Ampkα1 and promote M-MDSC-to-TAM differentiation. Moreover, accumulation of anti-

inflammatory cytokines, IL-10 and TGF-β in the TME could modulate AMPK and regulate M-MDSC-to-TAM differentiation (36).

The immunosuppressive activity of MDSC is regulated in part through an increased co-expression of Arginase I and Nos2 and the production of peroxynitrite (6). Paradoxically, Nos2-dependent tumoricidal and immunogenic anti-tumor effects were induced in TIP-DCs following T-cell ACT (46). In addition, treatment of tumor-bearing mice with the synthetic double-stranded RNA analog Poly-I:C transformed MDSC into cells that produced higher levels of nitric oxide and exhibited cytotoxic activity against cancer cells (47). Similarly, our results demonstrate that *Prkaa1*^{KO} M-MDSC triggered direct anti-tumor cytotoxic actions in a Nos2-dependent manner. Also, the upregulation of Nos2 in *Prkaa1*^{KO} M-MDSC complements previous reports showing the inhibitory effect of AMPK on the expression of Nos2 in macrophages, myocytes, and adipocytes (48). An important question unaddressed by our results is how the expression of Nos2 in MDSC could elicit paradoxical immunosuppressive or cytotoxic anti-tumor effects. Although the mechanisms mediating these opposite processes remain unknown, it is conceivable that the availability of the amino acid L-arginine could play a role. In fact, the expression of Arginase I in tumor-MDSC decreases the availability of the amino acid L-Arginine (49), which uncouples Nos2 to generate peroxynitrite rather than nitric oxide (50). Because we observed a dramatic decrease in the expression of Arginase I correlating with higher levels of Nos2 in *Prkaa1*^{KO} MDSC, it is possible that the production of immunosuppressive peroxynitrite in M-MDSC is replaced for tumor-cytotoxic nitric oxide. This prediction remains to be tested.

In summary, our results demonstrate the primary role of AMPKα1 in the immunosuppressive activities induced by tumor-MDSC; and provide strategies to overcome MDSC-driven T-cell dysfunction in tumors, which could enhance the effects of different forms of immunotherapy.

Supplementary Material

Refer to Web version on PubMed Central for supplementary material.

Acknowledgments

Authors would like to thank J. Kroger from the Flow Cytometry core; S. McCarthy from the CLIA Tissue Imaging core, and Janis De la Iglesia, PhD for their insightful advice. This work was partially supported by R01-CA184185 and R01-CA233512 to P.C.R.; and R01-CA157664, R01-CA124515, R01-CA178687, R01-CA211913 and U01-CA232758 to JRCG. Support for shared resources was provided by Cancer Center Support Grant (CCSG) CA076292 to H. Lee Moffitt Cancer Center.

Financial support: This work was partially supported by R01-CA184185 and R01-CA233512 to P.C.R.; and R01-CA157664, R01-CA124515, R01-CA178687, R01-CA211913 and U01-CA232758 to JRCG. Support for shared resources was provided by Cancer Center Support Grant (CCSG) CA076292 to H. Lee Moffitt Cancer Center.

Abbreviations:

ACT	Adoptive T-cell therapy
Aica-R	5-Aminoimidazole-4-carboxamide 1-β-D-ribofuranoside

Ampkα	AMP-activated protein kinase α
CAMKK2	calcium/calmodulin-dependent kinase kinase 2
CC	compound C
G-CSF	granulocyte colony-stimulating factor
GM-CSF	granulocyte-monocyte colony-stimulating factor
LLC	Lewis lung carcinoma
LKB1	liver-kinase-B1
TES	LLC tumor explants
L-NIL	Lysine dihydrochloride
L-NMMA	L-NG-Monomethylarginine
MDSC	Myeloid-derived suppressor cells
PMN-MDSC	granulocytic
M-MDSC	monocytic
Nos2	nitric oxide synthase 2
PNT	peroxynitrite
ROS	reactive oxygen species
Stat-5	signal transduction and activator of transcription 5
TAM	tumor-associated macrophages
TME	tumor microenvironment

References

1. Takizawa H, Boettcher S, Manz MG. Demand-adapted regulation of early hematopoiesis in infection and inflammation. Blood. 2012;119:2991–3002. [PubMed: 22246037]
2. Binnewies M, Roberts EW, Kersten K, Chan V, Fearon DF, Merad M, et al. Understanding the tumor immune microenvironment (TIME) for effective therapy. Nat Med. 2018;24:541–50. [PubMed: 29686425]
3. Bronte V, Brandau S, Chen SH, Colombo MP, Frey AB, Greten TF, et al. Recommendations for myeloid-derived suppressor cell nomenclature and characterization standards. Nat Commun. 2016;7:12150. [PubMed: 27381735]
4. Veglia F, Perego M, Gabrilovich D. Myeloid-derived suppressor cells coming of age. Nat Immunol. 2018;19:108–19. [PubMed: 29348500]
5. Fleming V, Hu X, Weber R, Nagibin V, Groth C, Altevogt P, et al. Targeting Myeloid-Derived Suppressor Cells to Bypass Tumor-Induced Immunosuppression. Front Immunol 2018;9:398. [PubMed: 29552012]
6. Gabrilovich DI, Ostrand-Rosenberg S, Bronte V. Coordinated regulation of myeloid cells by tumours. Nat Rev Immunol. 2012;12:253–68. [PubMed: 22437938]

7. Movahedi K, Laoui D, Gysemans C, Baeten M, Stange G, Van den Bossche J, et al. Different tumor microenvironments contain functionally distinct subsets of macrophages derived from Ly6C(high) monocytes. Cancer Res. 2010;70:5728–39. [PubMed: 20570887]
8. Franklin RA, Liao W, Sarkar A, Kim MV, Bivona MR, Liu K, et al. The cellular and molecular origin of tumor-associated macrophages. Science. 2014;344:921–5. [PubMed: 24812208]
9. Corzo CA, Condamine T, Lu L, Cotter MJ, Youn JI, Cheng P, et al. HIF-1alpha regulates function and differentiation of myeloid-derived suppressor cells in the tumor microenvironment. J Exp Med. 2010;207:2439–53. [PubMed: 20876310]
10. Garcia D, Shaw RJ. AMPK: Mechanisms of Cellular Energy Sensing and Restoration of Metabolic Balance. Mol Cell. 2017;66:789–800. [PubMed: 28622524]
11. Vaibhav K, Braun M, Khan MB, Fatima S, Saad N, Shankar A, et al. Remote ischemic post-conditioning promotes hematoma resolution via AMPK-dependent immune regulation. J Exp Med. 2018;215:2636–54. [PubMed: 30190288]
12. Sag D, Carling D, Stout RD, Suttles J. Adenosine 5'-monophosphate-activated protein kinase promotes macrophage polarization to an anti-inflammatory functional phenotype. J Immunol. 2008;181:8633–41. [PubMed: 19050283]
13. Hawley SA, Fullerton MD, Ross FA, Schertzer JD, Chevtzoff C, Walker KJ, et al. The ancient drug salicylate directly activates AMP-activated protein kinase. Science. 2012;336:918–22. [PubMed: 22517326]
14. Woods A, Dickerson K, Heath R, Hong SP, Momcilovic M, Johnstone SR, et al. Ca2+/calmodulin-dependent protein kinase kinase-beta acts upstream of AMP-activated protein kinase in mammalian cells. Cell Metab. 2005;2:21–33. [PubMed: 16054096]
15. Kim SJ, Tang T, Abbott M, Viscarra JA, Wang Y, Sul HS. AMPK Phosphorylates Desnutrin/ATGL and Hormone-Sensitive Lipase To Regulate Lipolysis and Fatty Acid Oxidation within Adipose Tissue. Mol Cell Biol. 2016;36:1961–76. [PubMed: 27185873]
16. Jeon SM, Chandel NS, Hay N. AMPK regulates NADPH homeostasis to promote tumour cell survival during energy stress. Nature. 2012;485:661–5. [PubMed: 22660331]
17. Rabinovitch RC, Samborska B, Faubert B, Ma EH, Gravel SP, Andrzejewski S, et al. AMPK Maintains Cellular Metabolic Homeostasis through Regulation of Mitochondrial Reactive Oxygen Species. Cell Rep. 2017;21:1–9. [PubMed: 28978464]
18. Al-Khami AA, Zheng L, Del Valle L, Hossain F, Wyczechowska D, Zabaleta J, et al. Exogenous lipid uptake induces metabolic and functional reprogramming of tumor-associated myeloid-derived suppressor cells. Oncoimmunology. 2017;6:e1344804. [PubMed: 29123954]
19. Li L, Wang L, Li J, Fan Z, Yang L, Zhang Z, et al. Metformin-Induced Reduction of CD39 and CD73 Blocks Myeloid-Derived Suppressor Cell Activity in Patients with Ovarian Cancer. Cancer Res. 2018;78:1779–91. [PubMed: 29374065]
20. Qin G, Lian J, Huang L, Zhao Q, Liu S, Zhang Z, et al. Metformin blocks myeloid-derived suppressor cell accumulation through AMPK-DACH1-CXCL1 axis. Oncoimmunology. 2018;7:e1442167. [PubMed: 29900050]
21. Kim SH, Li M, Trousil S, Zhang Y, Pasca di Magliano M, Swanson KD, et al. Phenformin Inhibits Myeloid-Derived Suppressor Cells and Enhances the Anti-Tumor Activity of PD-1 Blockade in Melanoma. J Invest Dermatol. 2017;137:1740–8. [PubMed: 28433543]
22. Uehara T, Eikawa S, Nishida M, Kunisada Y, Yoshida A, Fujiwara T, et al. Metformin induces CD11b+ cell-mediated growth inhibition of an osteosarcoma: implications for metabolic reprogramming of myeloid cells and antitumor effects. Int Immunol. 2018.
23. Ishii N, Matsumura T, Kinoshita H, Motoshima H, Kojima K, Tsutsumi A, et al. Activation of AMP-activated protein kinase suppresses oxidized low-density lipoprotein-induced macrophage proliferation. J Biol Chem. 2009;284:34561–9. [PubMed: 19843515]
24. Trikha P, Plews RL, Stiff A, Gautam S, Hsu V, Abood D, et al. Targeting myeloid-derived suppressor cells using a novel adenosine monophosphate-activated protein kinase (AMPK) activator. Oncoimmunology. 2016;5:e1214787. [PubMed: 27757311]
25. De Veirman K, Menu E, Maes K, De Beule N, De Smedt E, Maes A, et al. Myeloid-derived suppressor cells induce multiple myeloma cell survival by activating the AMPK pathway. Cancer Lett. 2019;442:233–41. [PubMed: 30419344]

26. Wu T, Zhao Y, Wang H, Li Y, Shao L, Wang R, et al. mTOR masters monocytic myeloid-derived suppressor cells in mice with allografts or tumors. Sci Rep. 2016;6:20250. [PubMed: 26833095]
27. Rong Y, Yuan CH, Qu Z, Zhou H, Guan Q, Yang N, et al. Doxorubicin resistant cancer cells activate myeloid-derived suppressor cells by releasing PGE2. Sci Rep. 2016;6:23824. [PubMed: 27032536]
28. Hammami I, Chen J, Murschel F, Bronte V, De Crescenzo G, Jolicoeur M. Immunosuppressive activity enhances central carbon metabolism and bioenergetics in myeloid-derived suppressor cells in vitro models. BMC Cell Biol. 2012;13:18. [PubMed: 22762146]
29. Svoronos N, Perales-Puchalt A, Allegrezza MJ, Rutkowski MR, Payne KK, Tesone AJ, et al. Tumor Cell-Independent Estrogen Signaling Drives Disease Progression through Mobilization of Myeloid-Derived Suppressor Cells. Cancer Discov. 2017;7:72–85. [PubMed: 27694385]
30. Roby KF, Taylor CC, Sweetwood JP, Cheng Y, Pace JL, Tawfik O, et al. Development of a syngeneic mouse model for events related to ovarian cancer. Carcinogenesis. 2000;21:585–91. [PubMed: 10753190]
31. Sierra RA, Trillo-Tinoco J, Mohamed E, Yu L, Achyut BR, Arbab A, et al. Anti-Jagged Immunotherapy Inhibits MDSCs and Overcomes Tumor-Induced Tolerance. Cancer Res. 2017;77:5628–38. [PubMed: 28904063]
32. Bronte V, Chappell DB, Apolloni E, Cabrelle A, Wang M, Hwu P, et al. Unopposed production of granulocyte-macrophage colony-stimulating factor by tumors inhibits CD8+ T cell responses by dysregulating antigen-presenting cell maturation. J Immunol. 1999;162:5728–37. [PubMed: 10229805]
33. Morales JK, Kmieciak M, Knutson KL, Bear HD, Manjili MH. GM-CSF is one of the main breast tumor-derived soluble factors involved in the differentiation of CD11b-Gr1- bone marrow progenitor cells into myeloid-derived suppressor cells. Breast Cancer Res Treat. 2010;123:39–49.
34. Casacuberta-Serra S, Pares M, Golbano A, Coves E, Espejo C, Barquinero J. Myeloid-derived suppressor cells can be efficiently generated from human hematopoietic progenitors and peripheral blood monocytes. Immunol Cell Biol. 2017;95:538–48. [PubMed: 28108746]
35. Li W, Tanikawa T, Kryczek I, Xia H, Li G, Wu K, et al. Aerobic Glycolysis Controls Myeloid-Derived Suppressor Cells and Tumor Immunity via a Specific CEBPB Isoform in Triple-Negative Breast Cancer. Cell Metab. 2018.
36. Biswas SK. Metabolic Reprogramming of Immune Cells in Cancer Progression. Immunity. 2015;43:435–49. [PubMed: 26377897]
37. Cha JH, Yang WH, Xia W, Wei Y, Chan LC, Lim SO, et al. Metformin Promotes Antitumor Immunity via Endoplasmic-Reticulum-Associated Degradation of PD-L1. Mol Cell. 2018;71:606–20 e7. [PubMed: 30118680]
38. Zhu YP, Brown JR, Sag D, Zhang L, Suttles J. Adenosine 5'-monophosphate-activated protein kinase regulates IL-10-mediated anti-inflammatory signaling pathways in macrophages. J Immunol. 2015;194:584–94. [PubMed: 25512602]
39. Saeedi R, Parsons HL, Wambolt RB, Paulson K, Sharma V, Dyck JR, et al. Metabolic actions of metformin in the heart can occur by AMPK-independent mechanisms. Am J Physiol Heart Circ Physiol. 2008;294:H2497–506. [PubMed: 18375721]
40. Foretz M, Hebrard S, Leclerc J, Zarrinpashneh E, Soty M, Mithieux G, et al. Metformin inhibits hepatic gluconeogenesis in mice independently of the LKB1/AMPK pathway via a decrease in hepatic energy state. J Clin Invest. 2010;120:2355–69. [PubMed: 20577053]
41. Rena G, Pearson ER, Sakamoto K. Molecular mechanism of action of metformin: old or new insights? Diabetologia. 2013;56:1898–906. [PubMed: 23835523]
42. Zhang M, Zhu H, Ding Y, Liu Z, Cai Z, Zou MH. AMP-activated protein kinase alpha1 promotes atherogenesis by increasing monocyte-to-macrophage differentiation. J Biol Chem. 2017;292:7888–903. [PubMed: 28330873]
43. Strauss L, Sangaletti S, Consonni FM, Szebeni G, Morlacchi S, Totaro MG, et al. RORC1 Regulates Tumor-Promoting "Emergency" Granulo-Monocytopoiesis. Cancer Cell. 2015;28:253–69. [PubMed: 26267538]

44. Kumar V, Cheng P, Condamine T, Mony S, Languino LR, McCaffrey JC, et al. CD45 Phosphatase Inhibits STAT3 Transcription Factor Activity in Myeloid Cells and Promotes Tumor-Associated Macrophage Differentiation. Immunity. 2016;44:303–15. [PubMed: 26885857]

45. Van Overmeire E, Stijlemans B, Heymann F, Keirsse J, Morias Y, Elkrim Y, et al. M-CSF and GM-CSF Receptor Signaling Differentially Regulate Monocyte Maturation and Macrophage Polarization in the Tumor Microenvironment. Cancer Res. 2016;76:35–42. [PubMed: 26573801]

46. Marigo I, Zilio S, Desantis G, Mlecnik B, Agnellini AHR, Ugel S, et al. T Cell Cancer Therapy Requires CD40-CD40L Activation of Tumor Necrosis Factor and Inducible Nitric-Oxide-Synthase-Producing Dendritic Cells. Cancer Cell. 2016;30:377–90. [PubMed: 27622331]

47. Shime H, Matsumoto M, Seya T. Double-stranded RNA promotes CTL-independent tumor cytolysis mediated by CD11b(+)Ly6G(+) intratumor myeloid cells through the TICAM-1 signaling pathway. Cell Death Differ. 2017;24:385–96. [PubMed: 27834952]

48. Pilon G, Dallaire P, Marette A. Inhibition of inducible nitric-oxide synthase by activators of AMP-activated protein kinase: a new mechanism of action of insulin-sensitizing drugs. J Biol Chem. 2004;279:20767–74. [PubMed: 14985344]

49. Rodriguez PC, Quiceno DG, Zabaleta J, Ortiz B, Zea AH, Piazuelo MB, et al. Arginase I production in the tumor microenvironment by mature myeloid cells inhibits T-cell receptor expression and antigen-specific T-cell responses. Cancer Res. 2004;64:5839–49. [PubMed: 15313928]

50. Xia Y, Zweier JL. Superoxide and peroxynitrite generation from inducible nitric oxide synthase in macrophages. Proc Natl Acad Sci U S A. 1997;94:6954–8. [PubMed: 9192673]

Statement of Significance. AMPK alpha-1 regulates the immunosuppressive activity and differentiation of tumor-MDSC, suggesting AMPK inhibition as a potential therapeutic strategy to restore protective myelopoiesis in cancer.

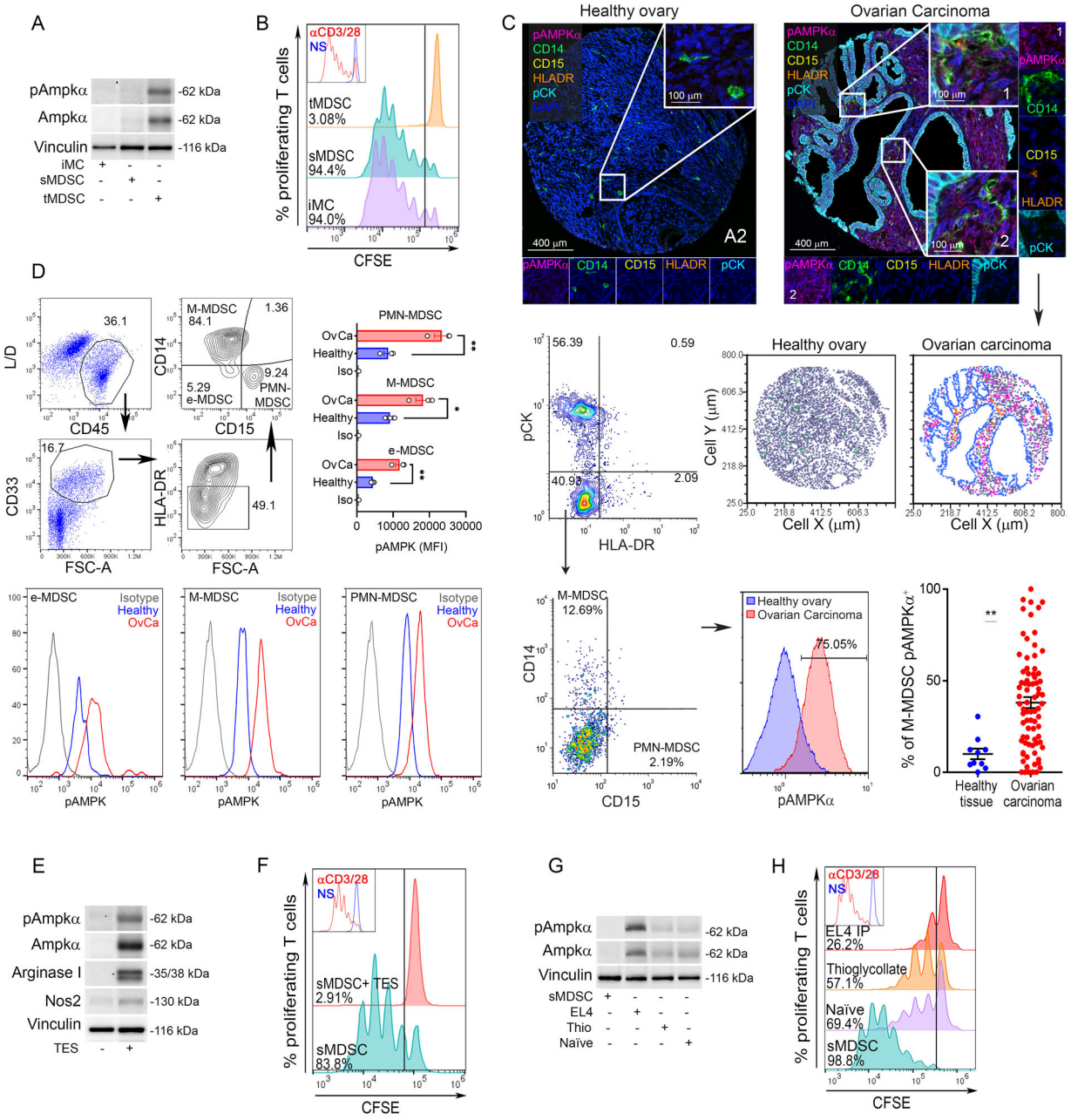

Figure 1. TME induces AMPKα in MDSC and boosts their immunoregulatory activity.

(A). Total and phospho-Ampkα in tumor-MDSC (tMDSC) and splenic-MDSC (sMDSC) from mice bearing LLC tumors, and in CD11b^{+} Gr1^{+} cells (iMC) from non-tumor bearing mice. Illustrative Immunoblot result from 5 mice.

(B) Representative result from 5 repeats showing the regulatory effect of tMDSC, sMDSC, and iMC on the proliferation of CFSE-labeled T-cells primed with plate-bound anti-CD3/CD28. T-cell proliferation was assessed 72 hours post-activation by flow cytometry. N=5.

(C). *Top*: Representative images (20x resolution and further 10x digital magnification) showing phospho-AMPKα (Magenta), CD14 (Green), CD15 (Yellow), HLA-DR (Orange), pan-Cytokeratin (pCK, Cyan), and DAPI (Blue) in a TMA containing healthy ovarian tissues

(N=10, *left*) and ovarian carcinoma tumors (N=79, *right*) by Vectra Automated Multispectral Imaging. *Middle right*: Representative cellular phenotype map showing the location of cells resembling M-MDSC (pCK^{neg} $HLA\text{-}DR^{neg}$ $CD14^{+}$ $CD15^{neg}$, green dots), phospho-AMPKα $^{+}$ M-MDSC (pink dots), monocytes-Dcs (pCK^{neg} $HLA\text{-}DR^{+}$ $CD14^{+}$ $CD15^{neg}$) (orange dots), pCK^{+} tumor cells (blue dots), and undefined stromal cells pCK^{neg} (grey dots). pCK^{neg} $HLA\text{-}DR^{neg}$ cells from ovarian tumors or healthy tissues (*Middle left)* were gated and plotted for CD14 (M-MDSC) or CD15 (PMN-MDSC) (*Bottom left*), and M-MDSC compared for phospho-AMPKα expression (*Bottom center*) and frequencies of phospho-AMPKα^{+} M-MDSC (*Bottom right*). Mean ± s.e.m.**$p < 0.01$ by unpaired Student's t-test.

(D) *Top-left*: Representative gating strategy for identification of e-MDSC, M-MDSC, and PMN-MDSC from peripheral blood of ovarian cancer patients and healthy controls. Merged (*Top-right*) and representative (*bottom*) phospho-AMPKα levels in MDSC subsets (N= 3/group).

(E). Total and phospho-Ampkα, Arginase I, and Nos2 in splenic-MDSC treated for 72 hours with 20% TES from primary LLC tumors. Representative immunoblot from 3 repeats.

(F). Anti-proliferative effect of MDSC from (E) on CFSE-labeled T-cells primed as in (B). N=3.

(G-H). $CD45.1^{+}$ sMDSC were transferred into: naïve $CD45.2^{+}$ mice, $CD45.2^{+}$ mice bearing i.p. $CD45.2^{+}$ EL4 tumors, or $CD45.2^{+}$ mice previously injected with thioglycolate. $CD45.1^{+}$ sMDSC were sorted 18 hours later. Representative results of total and phospho-Ampkα expression (G) and immunosuppressive activity on T-cells (H). N=4

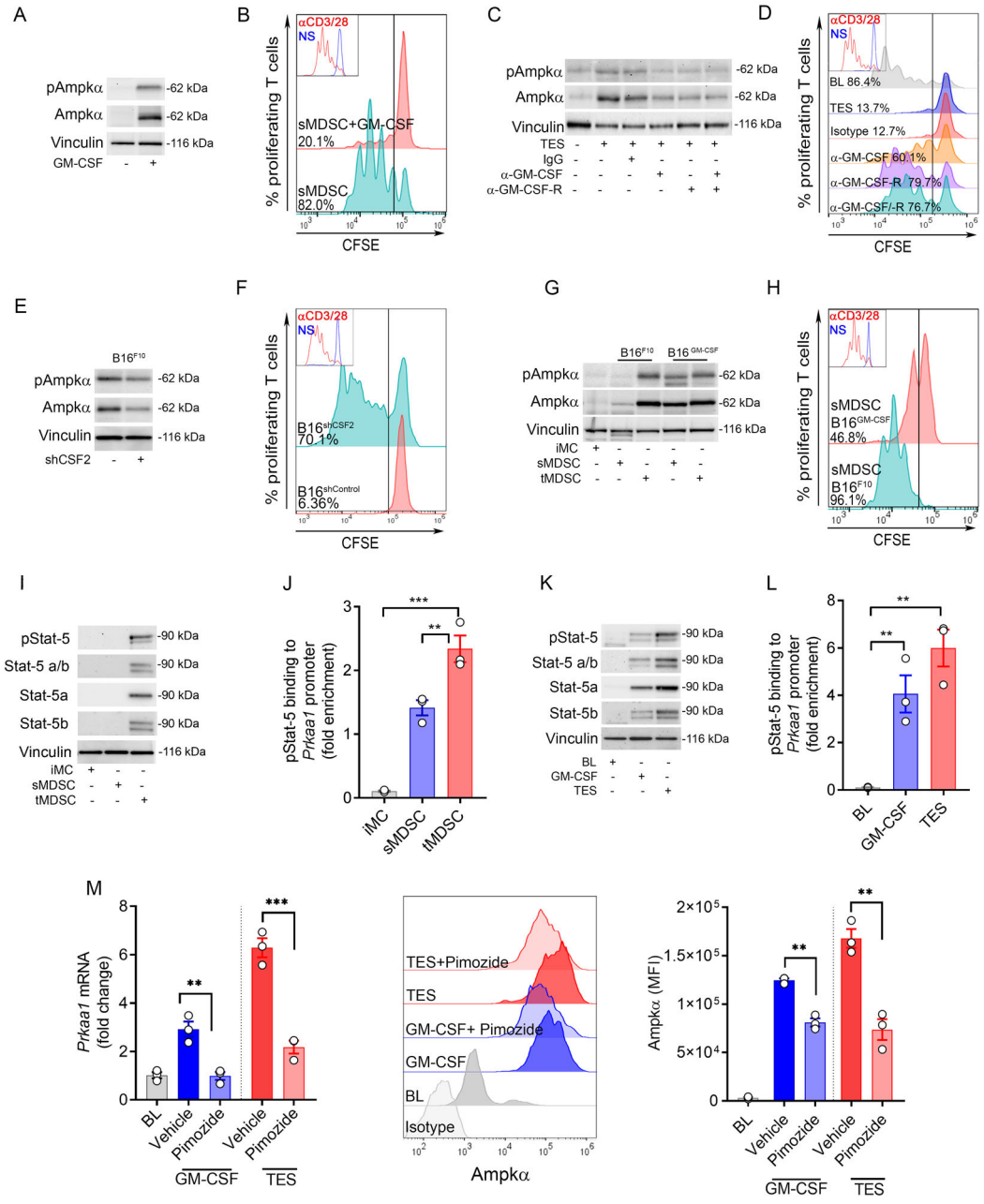

Figure 2. TME-associated GM-CSF triggers Ampkα expression in MDSC through Stat-5.

(A). Splenic-MDSC were isolated from LLC-bearing mice and treated for 72 hours with GM-CSF (20 ng/ml). Next, the expression of total and phospho-Ampkα was monitored. Results are a representative result from 3 independent experiments.

(B). MDSC from (A) were co-cultured with CFSE-labeled T-cells primed with anti-CD3/CD28. T-cell proliferation was tested 72 hours later by flow cytometry. Representative result from N=3.

(C-D). Splenic-MDSC from LLC-bearing mice were treated for 72 hours with 20% TES and in the presence of IgG isotype, anti-GM-CSF, and/or anti-GM-CSF-Rα. Total and phospho-

Ampkα expression (C) and capacity to block T-cell proliferation (D) were then assessed. Results are a representative illustration from 3 independent repeats.

(E-F). Tumor-MDSC from mice bearing B16 tumors previously transduced to express control or GM-CSF (*Csf2*)-targeting shRNA were tested for the expression of total and phospho-Ampkα and for the capacity to block T-cell proliferation. Results are representative from N=3.

(G). Representative result showing expression of total and phospho-Ampkα in iMC, or splenic-MDSC (sMDSC) and tumor-MDSC (tMDSC) from mice bearing s.c. B16-F10 or B16-GM-CSF tumors for 15 days. N=6 from 3 independent repeats.

(H). Splenic-MDSC from mice bearing similar sized B16-F10 or B16-GM-CSF tumors were tested for their ability to impair T-cell proliferation as in (B). Result is similar to 3 repeats.

(I). Expression of total Stat-5, Stat-5a, Stat-5b and phospho-Stat-5 in sMDSC and tMDSC from mice bearing s.c. LLC tumors, and iMC from spleens of tumor-free mice. N=3

(J). ChIP assay to detect endogenous binding of phospho-Stat-5 to *Prkaa1* promoter in cells from (I). Bars are Mean ± s.e.m. of 3 independent experiments. ***$p < 0.001$; **$p < 0.01$.

(K). Total Stat-5, Stat-5a, Stat-5b and phospho-Stat-5 in splenic-MDSC (BL) from LLC-bearing mice and treated for 72 hours with GM-CSF or 20% TES. Representative data from N=3.

(L). Endogenous binding of phospho-Stat-5 to *Prkaa1* promoter by ChIP assay in cells from (K). Bars are represented as Mean ± s.e.m. of 3 repeats. **$p < 0.01$.

(M). *Prkaa1* mRNA and AMPKα protein levels in baseline splenic-MDSC (BL) from LLC-bearing mice treated for 72 hours with GM-CSF or 20% TES in the presence of Stat-5 inhibitor, Pimozide (10 μM) or vehicle. Mean ± s.e.m. or representative of N=3. ***$p < 0.001$; **$p < 0.01$.

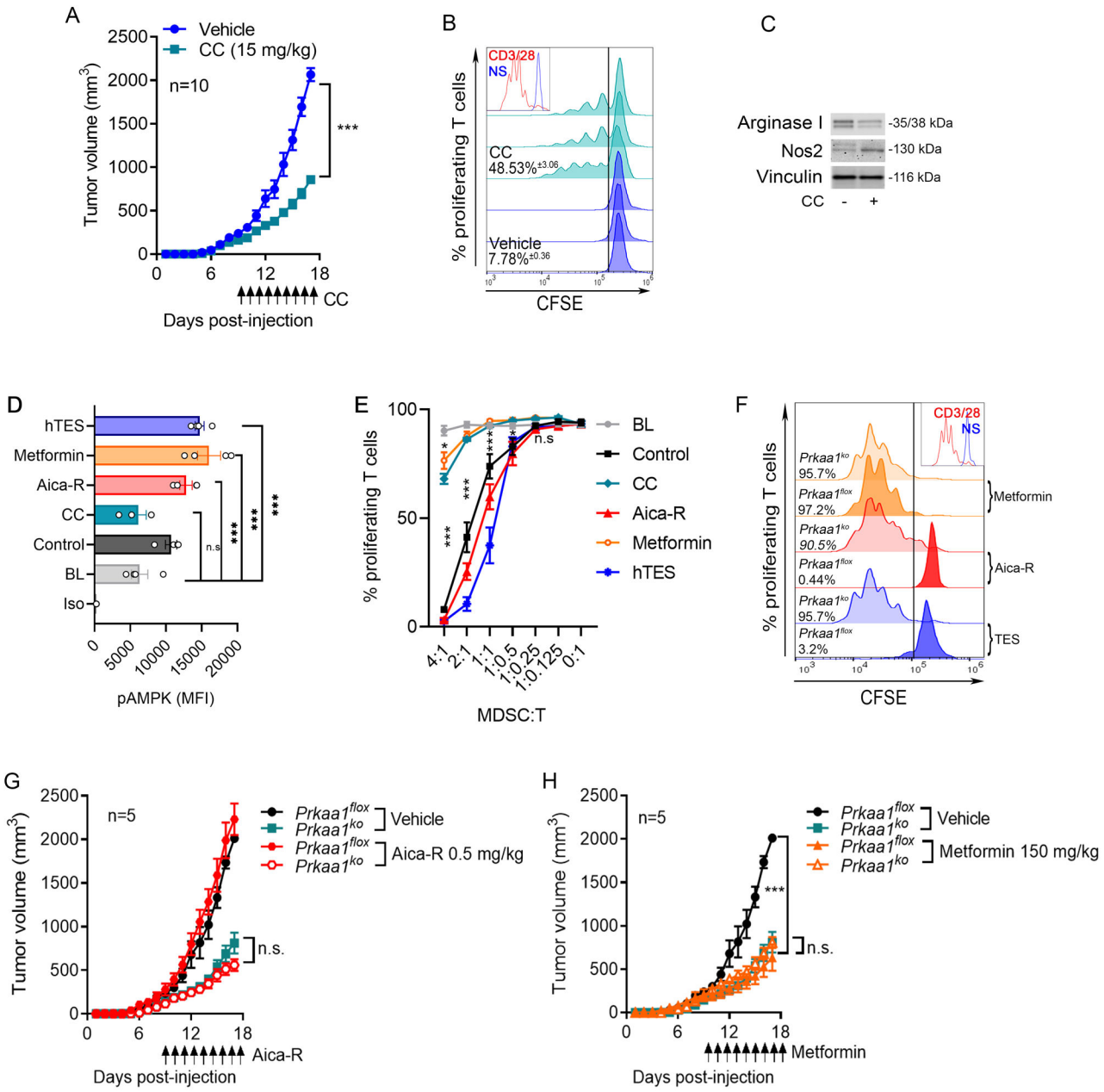

Figure 3. Ampk modulation regulates the immunosuppressive activity of tumor-MDSC.

(A). Tumor growth in LLC-bearing mice treated daily with CC, starting at day 9 post-tumor injection. Mean kinetics ± s.e.m of 7 mice/group in 2 repeats. ***$p < 0.001$

(B). Tumor-MDSC from LLC-bearing mice treated with CC or vehicle (day 17 post-tumor inoculation) were monitored for ability to blunt proliferation of CFSE-labeled T-cells primed with anti-CD3/CD28. Histograms show 3 repeats and percentages are Mean ± s.e.m.

(C). Arginase I and Nos2 levels in tumor-MDSC from (B). Representative result from N=3.

(D-E). Human MDSC developed after treatment of myeloid precursors with GM-CSF plus IL-6, and CC, Aica-R, Metformin, or 30% hTES for 7 days were tested for phospho-

AMPKα levels by flow cytometry (D) and for their ability to block proliferation of CFSE-labeled T-cells (anti-CD3/CD28) (E). N=3

(F). Splenic-MDSC from LLC-bearing flox and *Prkaa1*^{KO} mice were treated for 72 hours with 20% TES, Aica-R or Metformin and tested for the ability to block anti-CD3/CD28-induced T-cell proliferation. Representative finding from 3 repeats.

(G-H). Flox and *Prkaa1*^{KO} mice were injected with LLC tumors and 9 days later received daily treatments with Aica-R or Metformin. Tumor volume was tested until endpoint. N=10/group.

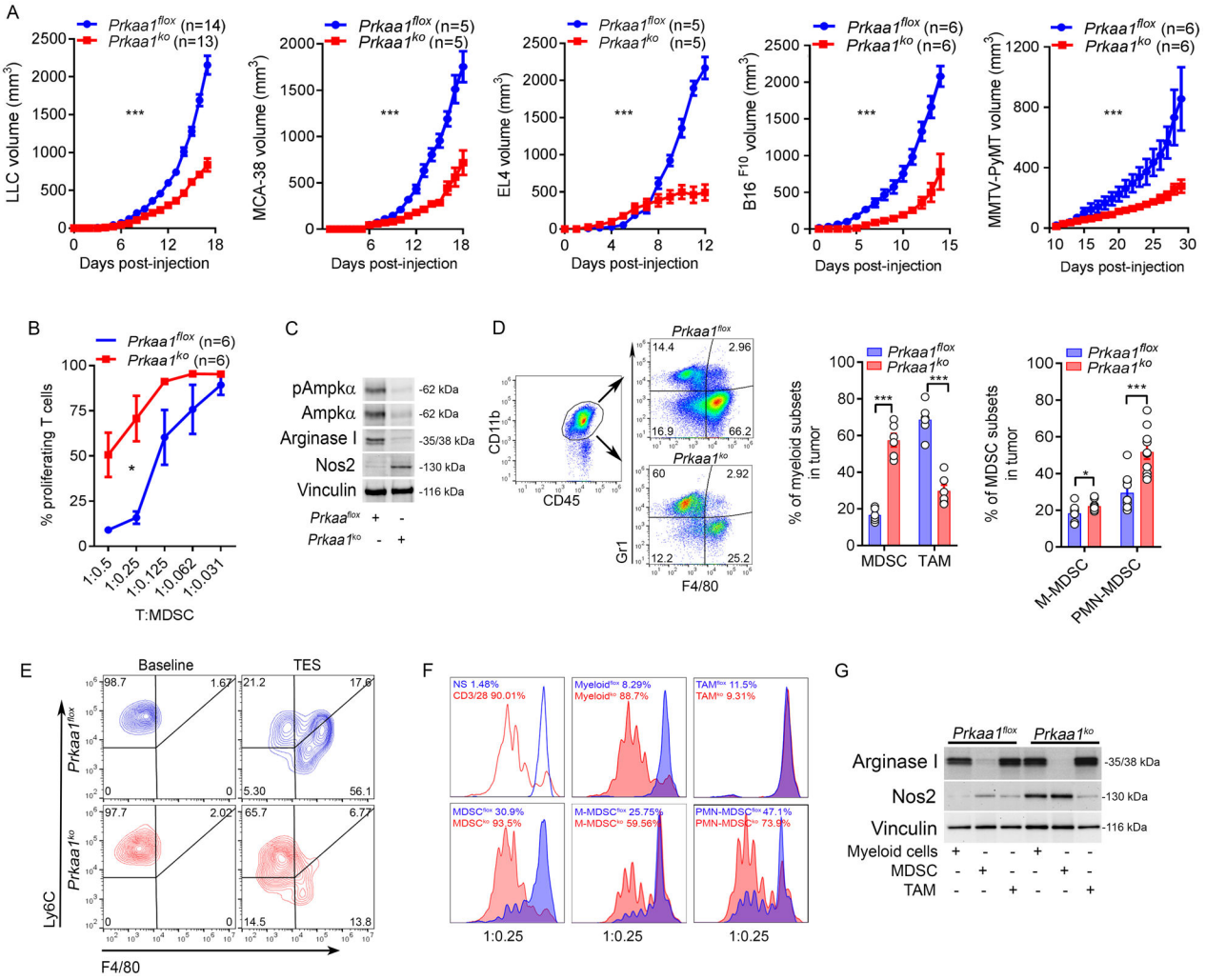

Figure 4. *Prkaa1* intrinsically regulates MDSC activity and differentiation.

(A). Flox and *Prkaa1*^{KO} mice were injected in 2 independent repeats with LLC (N=14), MCA-38 (N=5), EL4 (N=5), B16 (N=6), or MMTV-PyMT (N=6) tumors. Average kinetics ± s.e.m. ***p < 0.001.

(B-C). Tumor-MDSC were isolated from flox and *Prkaa1*^{KO} mice bearing LLC tumors for 17 days and tested for their ability to impair proliferation of CFSE-labeled T-cells primed with anti-CD3/CD28 (B), and for the expression of total and phospho-AMPKα, Arginase I, Nos2, and vinculin (C). Results are a representative finding from 6 mice/group and 2 independent repeats. *p < 0.05 by two-tailed unpaired Student's t-test.

(D). *Left*: strategy for evaluation of MDSC and TAM in tumors. Myeloid cells were gated based on CD11b^{+}, followed by discrimination of MDSC (CD45^{+} CD11b^{+} Gr1^{+} F4/80^{neg}) and TAM (CD45^{+} CD11b^{+} Gr1^{neg} F4/80^{+}). *Center*: MDSC and TAM frequency in LLC tumors from flox and *Prkaa1*^{KO} mice. N=6 from 2 independent studies. *Right*: PMN-MDSC (CD45^{+} CD11b^{+} Gr1^{+} Ly6C^{low} Ly6G^{+}) and M-MDSC (CD45^{+} CD11b^{+} Gr1^{+} Ly6C^{high} Ly6G^{neg}) in LLC tumors from flox and *Prkaa1*^{KO} mice. N=10 from 2 repeats. Bars are Mean ± s.e.m. ***p < 0.001, *p < 0.05.

(E). Flow cytometry sorted splenic-M-MDSC from flox and *Prkaa1*^{KO} mice bearing LLC tumors for 17 days were treated with 20% TES for 72 hours, after which their differentiation into TAM was evaluated by flow cytometry. N=3.

(F). Tumor-associated myeloid cells (CD11b^{+}), tumor-MDSC subsets and TAM were sorted by flow cytometry from flox and *Prkaa1*^{KO} mice bearing LLC tumors (17 days) and tested for ability to block T-cell proliferation as in (B). N=3 repeats.

(G). Representative expression of Arginase I and Nos2 by western blot in sorted cells from (F). Results are from 3 independent repeats.

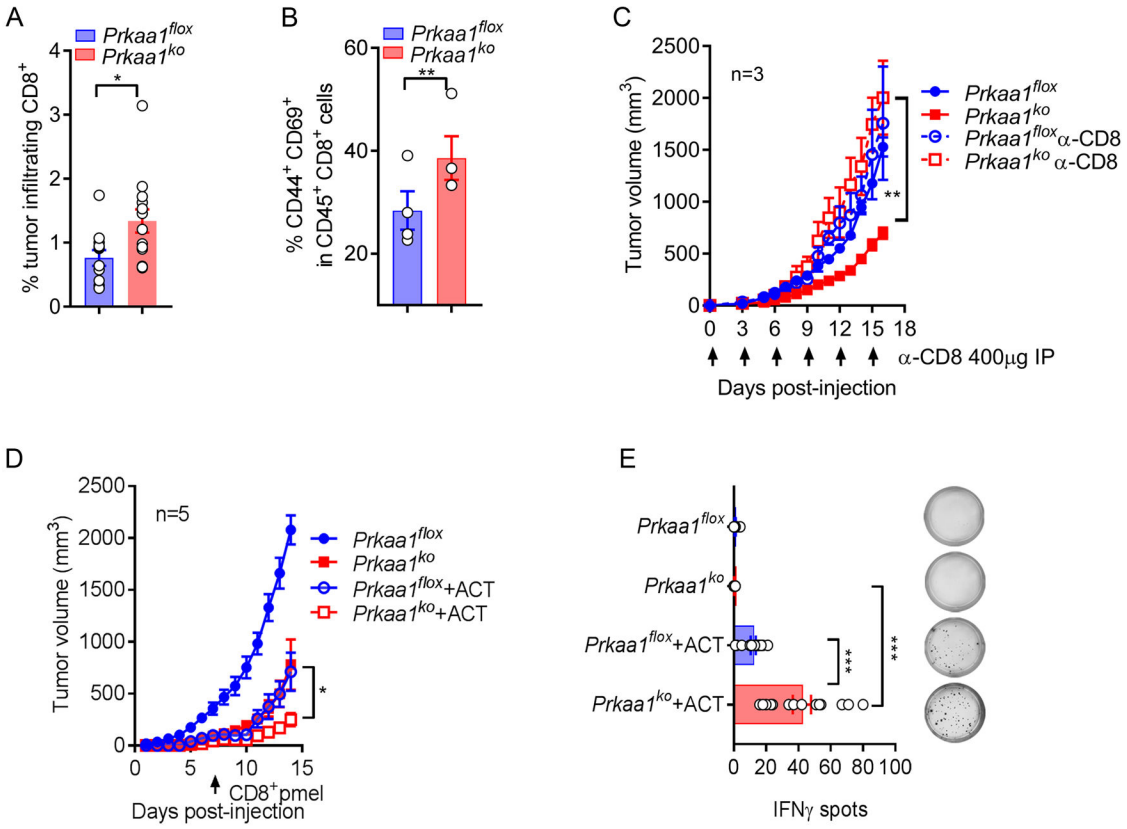

Figure 5. *Prkaa1* deletion in myeloid cells promotes anti-tumor T-cell immunity.

(A-B). Frequency of $CD45^+CD8^+$ (A) and antigen-experienced $CD44^+$ $CD69^+$ effector $CD8^+$ (B) T-cells was evaluated in LLC tumors from *Prkaa1*^{flox} or *Prkaa1*^{KO} mice. (N=13 tumors/group). Bar graphs are Mean ± s.e.m. and *p < 0.05, **p < 0.01 by two-tailed unpaired Student's *t*-test.

(C). LLC tumor growth in *Prkaa1*^{flox} (closed blue circle) or *Prkaa1*^{KO} (closed red square) mice, with or without 400 μg α-CD8 antibody injection on every 3rd day (open blue circle or open red square, respectively). Average tumor volume ± s.e.m in 3 mice/group. **p < 0.01 using unpaired Student's *t*-test.

(D). Flox and *Prkaa1*^{KO} mice were injected s.c. with B16 tumors and 6 days later, mice received $1X10^6$ $CD8^+$ Pmel T-cells primed with $gp100_{25–33}$ for 48 hours. Tumor volume was then monitored. Mean tumor volume ± s.e.m in 5 mice/group. *p < 0.05 by unpaired Student's *t*-test.

(E). Lymph nodes from flox or *Prkaa1*^{KO} mice bearing B16 tumors were collected 5 days after pmel T-cell transfer and evaluated for IFNγ production by EliSpot upon activation with $gp100_{25–33}$ for 24 hours. (N=3 repeats of 4 lymph nodes/group). Mean ± s.e.m. ***p < 0.001 using unpaired Student's *t*-test.

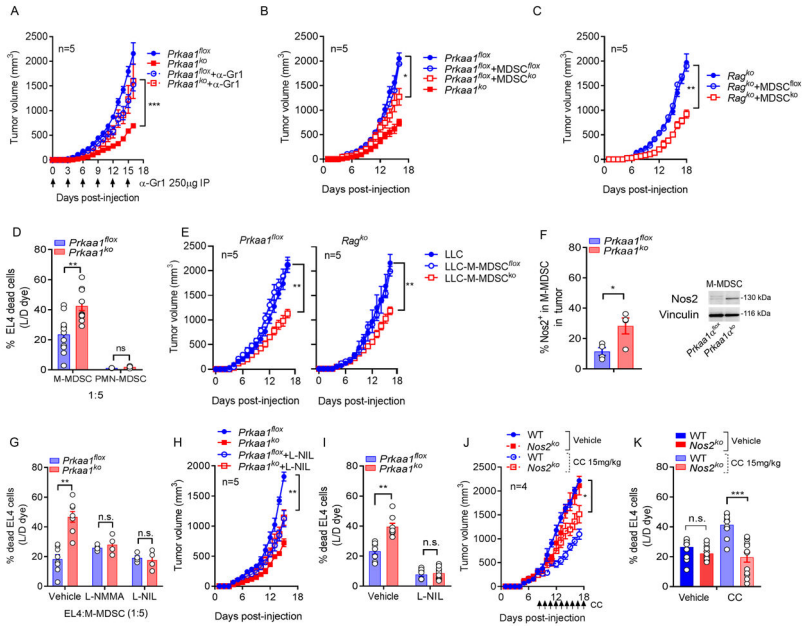

Figure 6. *Prkaa1*-deficient M-MDSC eliminate tumor cells in a Nos2-mediated manner.

(A). Tumor volume in flox or *Prkaa1*^{KO} mice bearing LLC tumors and treated or not with 250 μg anti-anti-Gr1 every 3rd day until tumor endpoint. N=5 per group. ***p < 0.001 by Student's *t*-test.

(B-C). Tumor growth in C57BL/6 (B) and immunodeficient *Rag*^{KO} (C) mice injected with LLC cells alone or co-injected at a 1:1 ratio with tumor-MDSC harvested from flox or *Prkaa1*^{KO} mice bearing LLC tumors. Mean ± s.e.m from 5 mice/group for B; and 3 mice/group for C. *p < 0.05; **p < 0.01 by Student's *t*-test.

(D). MDSC subsets were sorted from flox or *Prkaa1*^{KO} mice carrying s.c. LLC tumors for 17 days, and evaluated for their ability to kill EL4 tumors, as described in Methods. Bar graphs are Mean ± s.e.m of triplicates from 4 independent repeats. Ns > 0.05, **p < 0.01 by Student's *t*-test.

(E). Sorted tumor-M-MDSC from flox and *Prkaa1*^{KO} mice bearing LLC tumors for 17 days were co-injected at a 1:1 ratio with LLC cells into control (*left*) and *Rag*^{KO} (*right*) mice as in (B-C). Tumor volume was then assessed. N=5/group. **p < 0.01 by Student's *t*-test.

(F). Nos2 expression by flow cytometry (*left*) and western blot (*right*) in control and *Prkaa1*^{KO} M-MDSC sorted from mice bearing LLC-tumors. N=4. *p < 0.05.

(G) Cytotoxicity assay of M-MDSC on EL4 cells (D) was tested in the presence of the Nos2 inhibitors L-NMMA or L-NIL. Mean ± s.e.m of N=4. Ns > 0.05, **p < 0.01 by Student's *t*-test.

(H) Tumor growth in flox and *Prkaa1*^{KO} mice bearing LLC tumors treated daily with L-NIL (20 mg/kg, i.p.) or vehicle starting the day of tumor injection. Average tumor volume ± s.e.m in 5 mice/group. **p < 0.01 using unpaired Student's *t*-test.

(I). Tumor-M-MDSC were sorted from mice from (H) and evaluated for the ability to eliminate EL4 tumor cells *in vitro*. Mean ± s.e.m of triplicates of N=3. Ns > 0.05, **p < 0.01 by unpaired Student's *t*-test.

(J) Wildtype (WT) and *Nos2*^{KO} mice were injected with s.c. LLC tumors and treated 9 days later with CC (15 mg/kg, i.t.) or vehicle, as described in the Methods. Average tumor volume ± s.e.m in 4 mice/group. *$p < 0.05$ using unpaired Student's *t*-test.
(K). Tumor-M-MDSC sorted from mice from (I) were tested for the ability to kill EL4 tumor cells *in vitro*. Mean ± s.e.m of triplicates of N=4. Ns > 0.05, ***$p < 0.001$ by unpaired Student's *t*-test.